An Extended Field-Based Method for Noise Removal From Electron Tomographic Reconstructions

IEEE Access
Multidisciplinary | Rapid Review | Open Access Journal

Received January 1, 2018, accepted February 6, 2018, date of publication March 1, 2018, date of current version April 23, 2018.

Digital Object Identifier 10.1109/ACCESS.2018.2810866

An Extended Field-Based Method for Noise Removal From Electron Tomographic Reconstructions

FAISAL MAHMOOD[1,2], LARS-GÖRAN ÖFVERSTEDT[2], MÄRT TOOTS[2], GUNNAR WILKEN[2], AND ULF SKOGLUND[2]

[1]Department of Biomedical Engineering, Johns Hopkins University (JHU), Baltimore, MD 21218, USA
[2]Structural Cellular Biology Unit, Okinawa Institute of Science and Technology Graduate University (OIST), Okinawa 904-0412, Japan

Corresponding author: Faisal Mahmood (faisalm@jhu.edu)

This work was supported by the Japanese Government OIST Subsidy for Operations under Grant 5020S7010020. The work of F. Mahmood and M. Toots was supported by the OIST Ph.D. Fellowship. Ulf Skoglund and Gunnar Wilken are co-senior authors.

ABSTRACT Molecular structure determination is important for understanding functionalities and dynamics of macromolecules, such as proteins and nucleic acids. Cryo-electron tomography (ET) is a technique that can be used to determine the structures of individual macromolecules, thus providing the snapshots of their native conformations. Such 3-D reconstructions encounter several types of imperfections due to missing, corrupted, and low-contrast data. In this paper, we demonstrate that extending the reconstruction space, which increases the dimensionality of the linear system being solved during reconstruction, facilitates the separation of signal and noise. A considerable amount of the noise associated with collected projection data arises independently from the geometric constraint of image formation, whereas the solution to the reconstruction problem must satisfy such geometric constraints. Increasing the dimensionality thereby allows for a redistribution of such noise within the extended reconstruction space, while the geometrically constrained approximate solution stays in an effectively lower dimensional subspace. Employing various tomographic reconstruction methods with a regularization capability we performed extensive simulation and testing and observed that enhanced dimensionality significantly improves the accuracy of the reconstruction. Our results were validated with reconstructions of colloidal silica nanoparticles as well as *P. falciparum* erythrocyte membrane protein 1. Although the proposed method is used in the context of Cryo-ET, the method is general and can be extended to a variety of other tomographic modalities.

INDEX TERMS Cryo-electron microscopy, electron microscopy, electron tomography, tomography, denoising tomograms, extended field, ART, SIRT, Tikhonov regularization, maximum entropy tomography.

I. INTRODUCTION

Important functional information about biological macromolecules such as proteins and protein-nucleic acid complexes can be derived from their structures. However, most macromolecules, including proteins, are flexible, allowing them to interact dynamically with other molecules. Understanding such interactions has significant applications for drug development [1], [2]. Structure determination techniques are usually based on averaging methods such as x-ray diffraction (XRD), nuclear magnetic resonance (NMR) spectroscopy, or single particle cryo-electron microscopy. These techniques tend to lose information about structural flexibility and often require extensive sample purification. XRD also requires crystallization, which excludes a majority of biomolecules from this approach [3].

Cryo-electron tomography (Cryo-ET) is a method that can determine a plethora of 3D structures of individual biological molecules in their native states. It preserves the occurrence of many different molecular conformations due to rapid freezing at liquid nitrogen temperature. Since Cryo-ET does not necessarily require averaging [4], [5], it can provide vital information for examinations of proteins *in situ*, interactions among proteins, and analysis of molecular dynamics. Cryo-ET involves taking images of a cryo-specimen using a transmission electron microscope (TEM) at successive angles by tilting the specimen. These 2D images, often referred

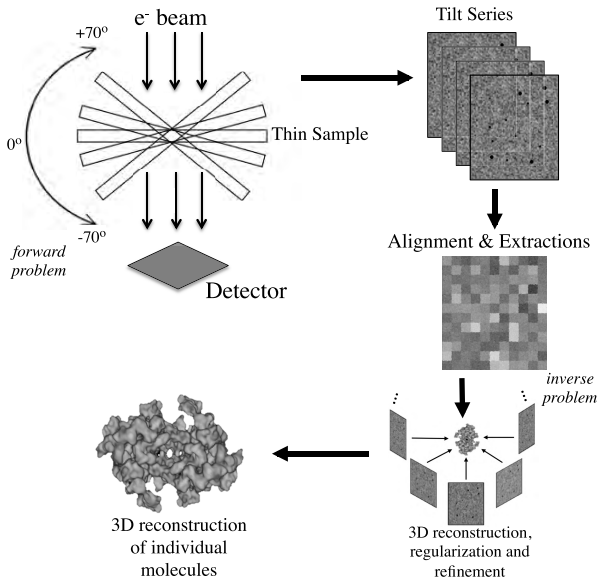

FIGURE 1. **The overall process of cryo-electron tomography from data collection (*forward problem*) to reconstruction and refinement (*inverse problem*).**

to as *tilt series*, are then aligned, and the desired region of reconstruction is extracted from each image. The 2D aligned extractions are then used to reconstruct a 3D tomogram via filtered back-projection (FBP) or other reconstruction and refinement methods [6], [7] (Fig. 1). The major challenge in Cryo-ET is to achieve reconstructions of single biological molecules at best possible resolution.

A. BACKGROUND

The theoretical resolution of tomographic reconstructions can be approximated by the optical thickness of the sample (D) and the number of equally spaced tilts (n, calculated over 180°) and is given by $R = \frac{\pi D}{n}$ [8]. However, this theoretical resolution is never achievable since 3D reconstruction from TEM images is a severely *ill-posed inverse problem*, encountering several challenges that stem from noisy and incomplete data. The data usually encounters several different types of imperfections and measurement errors [9]. First, 2D tilt images are usually collected at small angular differences. Ideally, tilts should be recorded to cover the entire 180° range of angles. However, the small space within the pole piece gap of the TEM objective lenses, where the specimen is placed, limits the tilt angle to about ±70°, which leads to missing data commonly known as the *missing wedge* [10]. Second, *specimen noise* occurs due to rearrangement of the specimen during data recording and to its degradation due to electron beam damage. Third, to minimize radiation damage, the sample is usually exposed to a low electron dose, which decreases the signal-to-noise ratio (SNR) of the micrographs. The low-dose causes uncorrelated *shot noise*, resulting from low illumination. Shot noise is usually Poisson-distributed and can be reduced using procedures of regularized refinement [7]. Fourth, during data acquisition, the specimen is tilted, and at every tilt angle θ, its effective thickness increases according to $1/\cos\theta$ [11]. This increased thickness causes more scattering, which contributes to low contrast in the image. Fifth, *correlated noise* can appear due to imperfections of the TEM detector. Normally, a gain reference is created to equalize the response from individual detector elements. However, errors in the gain reference give rise to noise that can be correlated with a region of the detector rather than with the specimen.

Several reconstruction methods have been employed over the years, but generally they can be divided into two categories: Fourier slice theorem-based analytical methods and regularizing methods that are often iterative. Analytical algorithms, such as filtered back projection (FBP) [12] have been extensively used for tomographic reconstructions. However, such algorithms usually need a large number of projections, and it is difficult to incorporate *a priori* information and additional constraints into the approximate solution. Electron lambda tomography (ELT) is another analytical method [13] useful if the ROI does not contain the whole object. When dealing with a reconstruction problem marred by missing and noisy data, regularizing methods are better suited. Among such methods, the mildly regularizing Algebraic Reconstruction Technique (ART) [14], Simultaneous Iterative Reconstruction Technique (SIRT) [15], and its variants [16], [17] are often classified as Algebraic Reconstruction Methods (ARMs) or Row Action Methods (RAMs), cf. [18], [6]. Extended Field Iterative Reconstruction Technique (EFIRT) [19], which is based on ART and was published in 1974, briefly showed that reconstructing 2D images from 1D projections within an extended field can lead to low noise in the region of interest (ROI) and fast convergence. However, [19] offers only limited experimental and empirical evidence of the method. Algebraic methods have a limited regularization capability. This problem can be addressed by the use of variational regularization methods such as Tikhonov regularization [20] and Constrained Maximum Entropy Tomography (COMET) [7] that are equipped with explicit regularization and goodness-of-fit constraints. Other modern methods include sparsity exploiting interior tomography and compressed sensing methods such as ICON [21] and others [11], [22]–[24]. Besides compressed sensing such methods usually also rely on variational regularization-based methods to increase sparsity.

COMET is an iterative reconstruction algorithm that performs a deconvolution of the point spread function (PSF), cf. [9], and enhances the contrast and resolution specifically for Cryo-ET by increasing the SNR. This was first published in 1996 by Skoglund *et al.* [7], mathematically analyzed by Rullgård *et al.* [25], and has been extensively used for structure determination, e.g. in [26], [27], and [28]. COMET can improve the fidelity of 3D reconstructions by reducing the shot noise. It increases (theoretically maximizes) the entropy relative to a prior obtained in the first iteration step from FBP, while iteratively deconvolving the PSF. In each iteration step it projects the new density to obtain virtual projections which are then

compared to the original tilts using a Chi-squared goodness-of-fit statistic in order to find an optimal balance between relative entropy and goodness-of-fit. A plethora of modern image reconstruction methods developed for CT, PET and SPECT are not directly applicable to Cryo-ET because of extreme low dose conditions. Moreover, certain learning and model-based methods can only be applied to reconstruction problems that focus on imaging similar specimens every time.

B. CONTRIBUTIONS

In 1974 Crowther and Klug [19] observed that extending the reconstruction space during ART reconstructions allows noise to spread out of the ROI. In this paper, inspired by [19], we further build on this idea by contributing the following:

- With extensive empirical experiments we demonstrate that extended field can go beyond ART and can be used to enhance a variety of reconstruction methods. We reconstructed several 2D phantoms from 1D projections corrupted with noise using ART (Kaczmarz, Symmetric Kaczmarz, Randomized Kaczmarz), SIRT (Cimmino, Landweber, DROP), and Tikhonov regularized reconstruction, and we observed that enhanced dimensionality resulting from a larger reconstruction space achieved higher correlation with the original phantom in every case.
- We verify how this method works by quantifying the amount of noise removed corresponding to the amount of noise added during simulations.
- We show that an extended field leads to better results when compared to non-extended reconstructions, and that it achieves this at a lower regularization parameter, thus preserving a better fit with the actual data and preventing over-smoothing.
- With extensive empirical simulations we show how extended field behaves at increasing extension steps.
- We further tested these effects on real Cryo-ET data, reconstructing the structure of colloidal silica as well as reconstructing a single *PfEMP1*-molecule from biological low-dose data using COMET and observed that an extended field renders low-noise reconstructions.
- We also explain the limitations of this method.

II. PROPOSED METHOD & SIMULATION EXPERIMENTS

In order to analyze the *ill-posed inverse problem* of reconstructing data from projections (tilt-series), it is fundamental to have an accurate formulation of the *forward operator*, solving the problem of modelling the process of image formation in the absence of noise and measurement errors [3]. Mathematically, a discretized and simplified version of the noise-free forward operator can be described in terms of a linear system where projections b are collected from object x, given a matrix representation of the imaging device A.

$$Ax = b \quad A \in \mathbb{R}^{m\times n} \;\; x \in \mathbb{R}^n \;\; b \in \mathbb{R}^m \tag{1}$$

The sinogram (S) represents the tilt series of raw data, *i.e.*, a matrix where each column represents a projection at a different angle. The vector b is the vectorized form of S. Each row of A corresponds to a single ray passing through the density being imaged. Since each ray only passes through a certain number of voxels, matrix A is usually sparse. This sparsity can be used to a computational advantage since A can be stored and used in a sparse way, utilizing less memory. The forward model presented here is rather primitive and has been introduced for the purposes of simulation and testing. A more detailed account of the forward model for ET has been given in [9].

The imaging model presented above represents a set of linear equations such that there is one equation for each ray passing through the object. Each equation here can be considered as a hyperplane in vector space, which can be defined as $\mathcal{H}_i = \{x \mid a_i^T x = b_i\}$. In an ideal, noise-free case, these linear equations would be consistent, and a solution would exist at the intersection of these hyperplanes. For the purpose of demonstration this has been shown for a system of two linear equations (Fig. 2a). However, in practice this is never the case, since the right hand side of the linear system is usually marred by noise $b = b^* + e$, where b^* is ideal data and e represents perturbation or data error. This renders the system inconsistent, and for algebraic techniques an approximate solution is sought within the region enclosed by the hyperplanes rather than at their intersection (Fig. 2b). Ill-posed inverse problems are generally not stable, *i.e.*, small perturbations in data can lead to large errors in the solution [29]. Hence, regularization methods are required to compute approximate solutions that are much less sensitive to perturbations in b [29]. Tikhonov regularization is a classical method of reducing the sensitivity of the solution to perturbations and noise in acquired data. The Tikhonov regularized solution can be defined as the solution to the following problem, see [20], [30]:

$$\min_x \{\|Ax - b\|_2^2 + \lambda^2 \|x\|_2^2\} \tag{2}$$

$\|Ax - b\|_2^2$ measures the goodness-of-fit which essentially measures the effectiveness of the solution while the second term, $\|x\|_2^2$, measures the regularity of the solution, *i.e.*, it controls the norm of x in order to suppress large noise components. The optimal balance between the two terms is weighted by the regularization parameter, λ. For a large λ, more weight is given to the minimization of the solution norm $\|x\|_2^2$ which then produces a more regular solution. For small values of λ the solution tends to be less smooth since more weight is given to fitting the noisy data.

Extended Reconstructions: Extended reconstruction essentially means reconstructing within a region larger than the region of interest (ROI). *This region outside the ROI gives extra freedom and flexibility to minimize data discrepancies and to maximize the consistency of the reconstruction within the ROI, with respect to the projections* (Fig. 2c). Moreover, since we do not impose a non-negativity constraint in the extra region around the ROI, this essentially allows an extra degree of freedom when fitting the projections from our reconstruction to the sinogram.

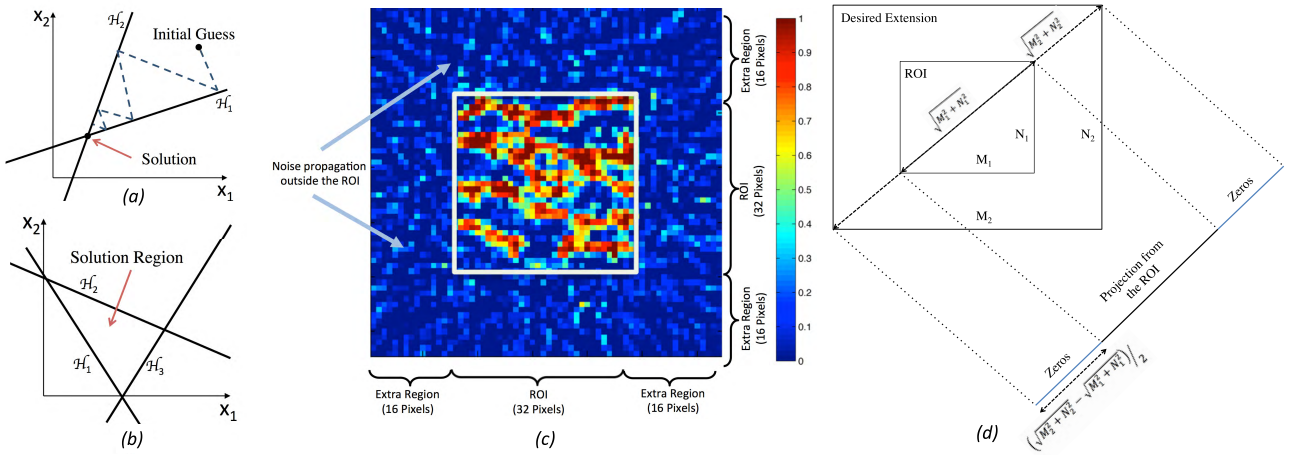

FIGURE 2. a) Consistent System of Equations having an exact solution, showing how Kaczmarz method approaches the solution starting from an initial guess. b) In case of an inconsistent noisy system the solution would be in a region bound by hyperplanes rather than at their intersection. c) Reconstruction of a binary phantom with an extra region larger than the ROI. Unconstrained noise is redistributed out of the geometrically constrained ROI. The extra region gives flexibility to minimize data errors and maximize consistency of the solution within the ROI. d) Image showing how the sinogram is extended to achieve an extra region outside the ROI. If a sinogram corresponding to a $N_1 \times M_1$ phantom is to be extended to a reconstruction corresponding to $N_2 \times M_2$, the sinogram is extended by zero-padding each projection with $(\sqrt{M_2^2+N_2^2}-\sqrt{M_1^2+N_1^2})/2$ on each side. For example, if the sinogram of a 64 × 64 phantom is extended to a 128 × 128 phantom the extension on each side of the sinogram would be 45.

A. ART WITH EXTENDED FIELD (EART)

According to ART (Kaczmarz method [31]) the solution to a linear system of equations can be estimated starting from an initial guess and orthogonally projecting it onto successive hyperplanes until a stopping criterion is met (Fig. 2a). However, in cases where the solution is inconsistent the introduction of a relaxation parameter γ can speed up convergence,

$$x^{k+1} = x^k + \gamma \frac{b_i - a_i^T x^k}{\|a_i\|_2^2} a_i \quad \gamma \in (0, 2). \tag{3}$$

The ideal relaxation parameter usually varies between $0 < \gamma < 2$ and is generally tuned to achieve best results [32]. There are various formulations of Kaczmarz method such as symmetric Kaczmarz [33] and randomized Kaczmarz [32]. Most of these formulations are based on the way the rows, i, of matrix A are accessed. Extended ART performs a reconstruction within a larger reconstruction space, which is achieved by extending the sinogram S, either by choosing a large reconstruction region or via zero-padding. Extending the sinogram via zero-padding means padding each individual projection with zeros on each side (Fig. 3, Step 3). If a sinogram corresponding to a $N_1 \times M_1$ phantom is to be extended to a reconstruction corresponding to $N_2 \times M_2$, the sinogram is extended by padding each projection with $(\sqrt{M_2^2+N_2^2}-\sqrt{M_1^2+N_1^2})/2$ zeros on each side. Extending the sinogram from a reconstruction size of $N \times M$ to $(N + e) \times (M + e)$ corresponds to an increased dimension of the sinogram from $\sqrt{N^2+M^2} \times n_\vartheta$ to $\sqrt{(N+e)^2+(M+e)^2} \times n_\vartheta$ where n_ϑ is the number of projections.

Extending the sinogram increases the dimensionality of the linear system $Ax = b$ and makes vector b more sparse. Having an extra region outside the ROI allows inconsistencies and noise to spread out into the extra region, minimizing the discrepancy and enabling the solution in the ROI to be more consistent. This means that when reconstructing with ART, Eq. 3 is applied to not only the required ROI, but to an extra region outside, thus rendering a large reconstruction

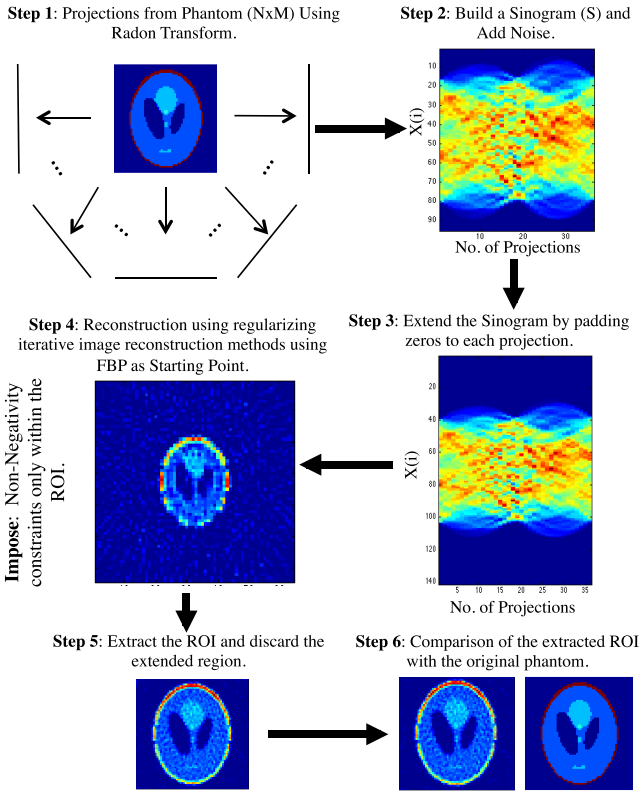

FIGURE 3. Flow diagram showing the simulation setup for extended field simulations with several different iterative reconstruction methods.

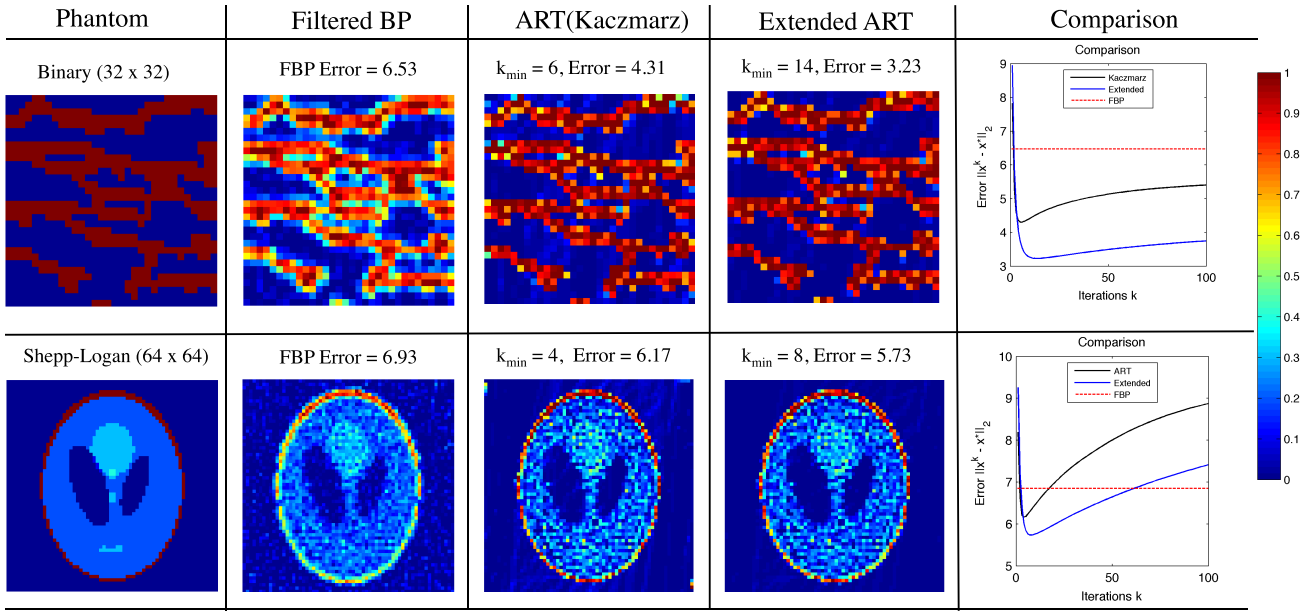

FIGURE 4. Comparative analysis of reconstructing a binary (relative noise = 0.05) and Shepp-Logan (relative noise = 0.1) phantom with ART and EART shows that EART can achieve a relatively lower error rate. More results with varying noise levels and number of projections have been presented in the supplement with this paper. Iterative image reconstruction videos showing noise being redistributed in the extended region can be viewed in the multimedia supplement with this paper.

where the region of interest is preserved and noise can redistribute to the extra region. On removing the extra region, inconsistent discrepancies are removed and the consistent solution is isolated. The density in the extra region originating from inconsistencies, noise, and fringe effects can be positive or negative; hence, the non-negativity constraint often used during ART should not be applied in the extra region.

B. SIMULATIONS WITH EART

Experiment I: To test the procedure defined in the previous subsection a 32 × 32 binary phantom [32] (x^*) was used. A sinogram was created by taking projections at every 5 degree starting from 1° to 180° (*i.e.*, $\theta = 1 : 5 : 180$). The projections were corrupted with a mixture of random Gaussian and Poisson noise (relative level = 0.05). This was done to simulate the Poisson shot noise and Gaussian electronic and dynamic range noise. This sinogram was then reconstructed using all three variants of ART. A version with an extended field (EART) was also reconstructed using all three ART procedures. The EART reconstructions were performed by increasing the dimensions of the sinogram corresponding to a 64 × 64 reconstruction. The error rate for the k^{th} iteration relative to the original phantom was calculated using $\left\|x^k - x^*\right\|_2$, where x^* is the original phantom and x^k is the result of the k^{th} iteration of the iterative method being used. The SNR for the reconstructions can be estimated using $SNR = \|x^*\|_2 / \left\|x^k - x^*\right\|_2$. It should be noted here that the error rate or SNR for extended reconstructions is always calculated corresponding to the ROI excluding the extended region. The complete experimental setup is shown in Fig. 3. These simulations were conduced using MATLAB R2016a. Zero-padding is only required when there is not enough region to reconstruct within the raw data. This is always the case for simulation studies conducted in this paper. However for real data when we are reconstructing a region rather than the entire data we can increase the volume of the reconstruction without zero-padding.

Experiment II: A 64×64 Shepp-Logan phantom [34] was used to further test the arguments presented at a higher noise level and the sinogram was corrupted by normalized noise of relative level 0.1. The EART reconstructions were performed by increasing the dimensions of the of the sinogram corresponding to a 128 × 128 reconstruction. The rest of the simulation setup is the same as experiment I.

Traditionally, Kaczmarz method and its variants show a semi-convergence behavior, where the first few iterations show a sharp decrease in error rate and then slow down, or in certain cases, diverge from the optimal solution. From the simulations it is evident that EART follows a similar trend. Although, EART needs more iterations to realize its full potential (Fig. 4), it gives a lower error at semi-convergence. While ART starts diverging from the solution, EART continues to reach semi-convergence in a later cycle, with a lower error-rate. These two experiments at relatively low and high noise, respectively, both show similar behavior and indicate that increasing the dimensionality of the reconstruction problem by increasing the reconstruction space has a direct effect towards improving reconstruction quality. Fig. 5a-f shows intensity profiles of a single line through each of the phantoms in experiments I and II. The X direction and Y direction indicate the horizontal and

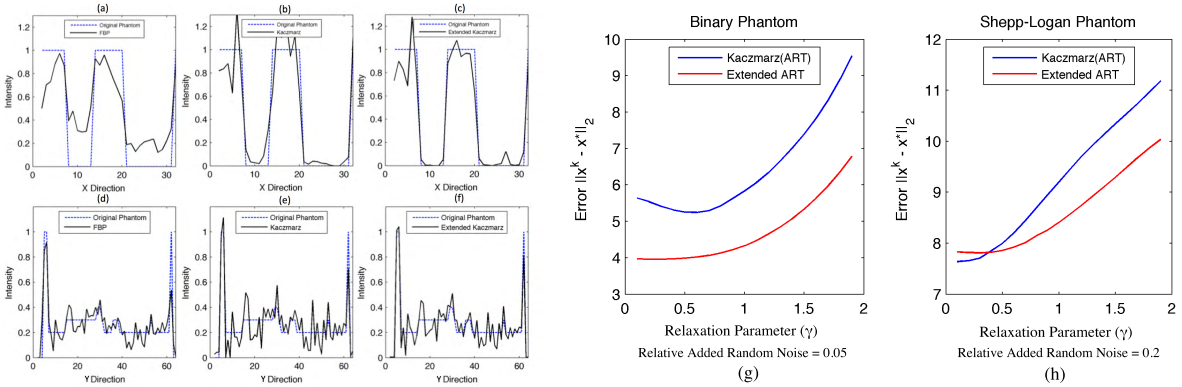

FIGURE 5. a-f) Intensity profiles of a line through the original and reconstructed binary and Shepp-Logan phantoms using FBP, ART (Kaczmarz) and EART (Extended Kaczmarz). The EART reconstructions show a relatively better fit to the original phantom as compared to ART reconstructions. g-h) Comparative analysis of ART and EART with respect to changing relaxation parameter γ.

TABLE 1. Comparison of error rates for ART and EART using various phantoms at 20% noise.

Phantom	FBP	Kaczmarz	Ex. Kaczmarz	Sym. Kaczmarz	Ex.Sym. Kaczmarz	Rand. Kaczmarz	Ex.Rand. Kaczmarz
Smooth	29.13	27.54	25.91	27.03	24.97	25.36	24.23
Shepp-Logan	13.98	10.21	9.78	10.32	9.61	10.16	9.01
Binary	11.04	8.40	7.51	8.98	7.83	8.36	7.12
Four-Phase	19.24	16.31	15.41	19.16	15.39	19.49	14.98

vertical direction in which the intensity profile was taken through the phantom. The difference between FBP, ART, and EART is evident. Simulation results with a much higher error rate (relative level = 0.20) have been summarized in Table 1.

Experiment III: In order to check the effect of the relaxation parameter γ, we performed several ART and EART reconstructions with varying γ between $0 < \gamma < 2$ (Fig. 5g-h). For both phantoms, the error rate is lower for EART reconstructions than for ART reconstructions, except at very low γ values, when the noise is relatively high. It should be be noted that the error reported here is the lowest error rate at semi-convergence.

C. SIRT WITH EXTENDED FIELD (ESIRT)

Unlike ART the class of SIRT methods are "simultaneous" which means that all rows of matrix A are used simultaneously in every iteration [32]. SIRT can thus perform faster than ART and has better regularization properties. SIRT class of methods can be generally defined as follows:

$$x^{k+1} = x^k + \gamma_k T A^T M(b - Ax^k) \tag{4}$$

Here x^k and x^{k+1} denote the current and successive iteration respectively. γ_k is the relaxation parameter, and the matrices M and T are symmetric positive definite. Various methods of SIRT have different M and T [35], [36]. Ideally, the iterations mentioned in Eq. 4 converge to a solution x^*. However, similar to ART this is usually not the case and the solution converges to a region and oscillates in this region over successive iterations. The class of SIRT methods also follow a semi-convergence behavior as shown in [37] and [38]. Similar to EART a version of SIRT can be formulated by extending the region outside the ROI either by zero-padding or within the region being reconstructed. This will lead to the enhanced dimensionality of the linear system being solved and extra reconstruction space, these extra dimensions act as a mechanism for segregating most of the background noise.

Simulation and testing was performed on three variants of SIRT, *i.e.*, Landweber, Cimmino and Diagonally Relaxed Orthogonal Projections (DROP). Landweber's method [39] simply originates from Eq. 4 where $M = I$ and $T = I$ and I represents an identity matrix. Cimmino's method [17] works on the premise that each iteration is the weighted average of the projections of the previous iteration on all the hyperplanes:

$$x^{k+1} = x^k + \gamma_k \frac{1}{m} \sum_{i=1}^{m} w_i \frac{b_i - \langle a_i, x^k \rangle}{\|a_i\|_2^2} a_i. \tag{5}$$

Where, w_i represents the weights. In terms of Eq. 4 Cimmino is defined as having $M = D$ and $T = I$, where D can be defined as follows:

$$D = \frac{1}{m} diag\left(\frac{w_i}{\|a_i\|_2^2} a_i \right). \tag{6}$$

DROP is an extension of Cimmino's original method and incorporates information about sparsity of matrix A [40]. When extending the dimensionality by adding an extra region outside the ROI the vector b is increased and becomes sparse. The extra region adds additional hyperplanes to the system

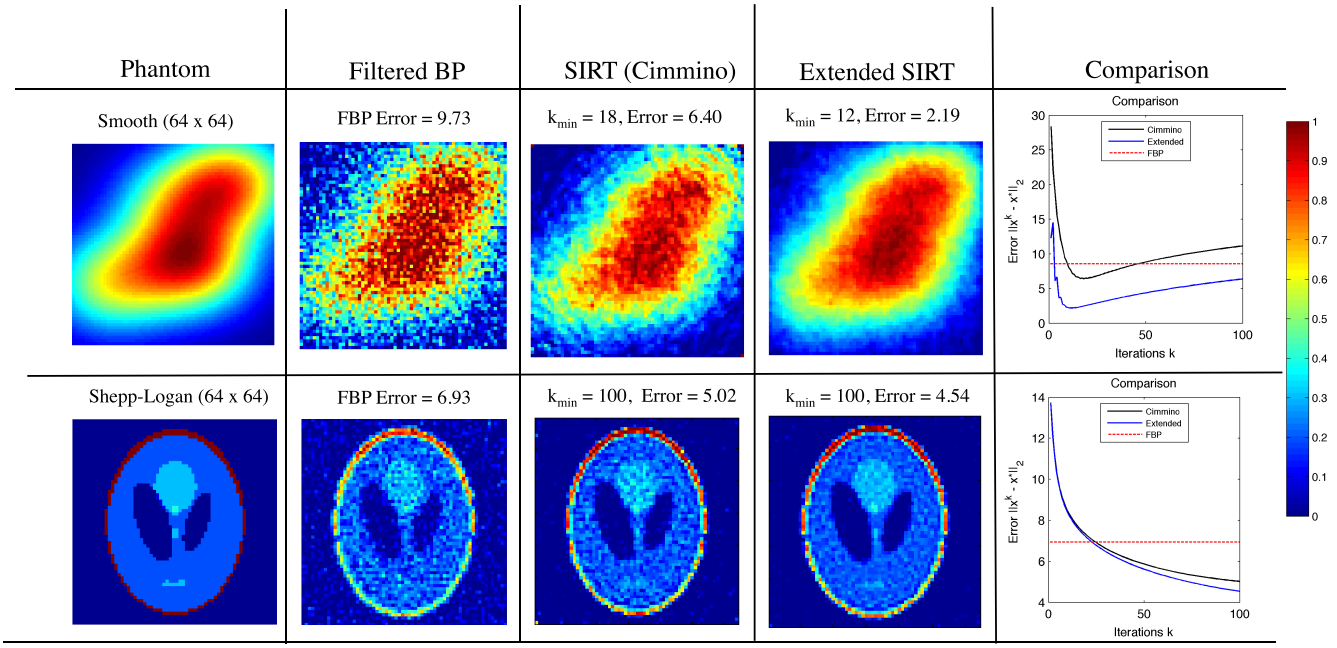

FIGURE 6. Comparative analysis of reconstructing a smooth phantom (relative noise = 0.05) and Shepp-Logan (relative noise = 0.1) with SIRT and ESIRT shows that ESIRT can achieve a lower error rate as compared to SIRT. More results with varying noise levels and number of projections have been presented in the supplement with this paper. Iterative image reconstruction videos showing noise being redistributed in the extended region can be viewed in the multimedia supplement with this paper.

passing through the origin. This essentially means that for Cimmino's method more hyperplanes are averaged to achieve the output of every iteration which in turn leads to distribution of noise to extra space. Similar to EART the solution stays in an effectively lower dimensional sub-space and the noise redistributes to higher dimensions.

D. SIMULATIONS WITH ESIRT

A 64 × 64 smooth [32] and Shepp-Logan [34] phantom was reconstructed using FBP, SIRT, and ESIRT with all three variants mentioned in the previous sub-section. Sinograms for these phantoms were created by taking projections every 5 degrees from 1° to 180° degrees (*i.e.*, $\theta = 1 : 5 : 180$) and corrupted with normalized noise relative level 0.05 for smooth and 0.1 for Shepp-Logan, respectively. ESIRT reconstructions were performed by increasing dimensions of the sinogram corresponding to a 128 × 128 reconstruction. Both iterative methods were stopped at 100 iterations (k). The error rate was calculated as mentioned in the previous sub-section. Fig. 6 shows a comparative analysis of SIRT and ESIRT methods in detail. Visual inspection of the reconstructed phantom shows that ESIRT has better regularization properties than SIRT. It is evident that ESIRT achieves a much better correlation with the original phantom as compared to SIRT. In the case of ESIRT, the divergence from semi-convergence is also slower. Fig. 7 shows an intensity profile of a single line through SIRT and ESIRT phantoms reconstructed using Cimmino's method and indicates that ESIRT behaves much better than SIRT. Simulations at a high noise level (relative level = 0.20) are presented in Table 2.

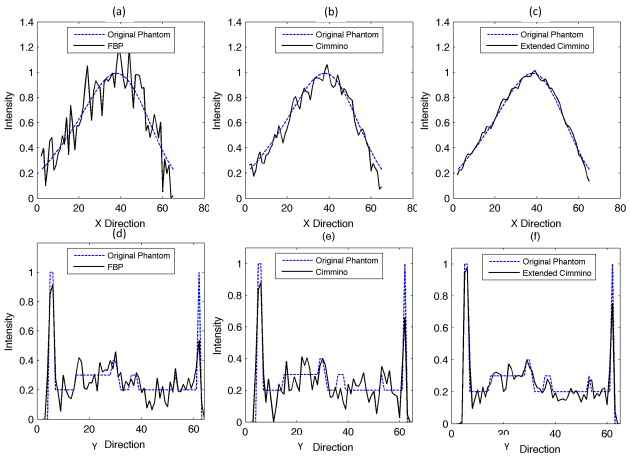

FIGURE 7. Intensity profiles of a line through the original and reconstructed smooth and Shepp-Logan phantoms using FBP, SIRT (Cimmino) and ESIRT (Extended Cimmino). The ESIRT reconstructions show a better fit to the original phantom as compared to SIRT reconstructions.

Details regarding the Four-Phase phantom used for this study can be found in [32].

E. SIMULATIONS WITH EXTENDED TIKHONOV REGULARIZATION (ETR)

Tikhonov Regularization (TR) has already been explained earlier, TR has a stronger regularization capability as compared to SIRT and ART and has been extensively used in the context of various *ill-posed inverse problems* [29]. We conducted several experiments to test the effectiveness of an

TABLE 2. Comparison SIRT and ESIRT using various phantoms at 20% noise.

Phantom	FBP	Cimmino	Ex.Cimmino	Landweber	Ex.Landweber	DROP	Ex.DROP
Smooth	29.13	23.26	21.70	23.43	20.11	23.41	20.32
Shepp-Logan	13.98	9.13	8.34	9.13	8.33	8.78	7.82
Binary	11.04	7.18	6.32	7.38	6.34	7.09	6.28
Four-Phase	19.24	13.96	12.44	13.77	12.19	13.63	11.91

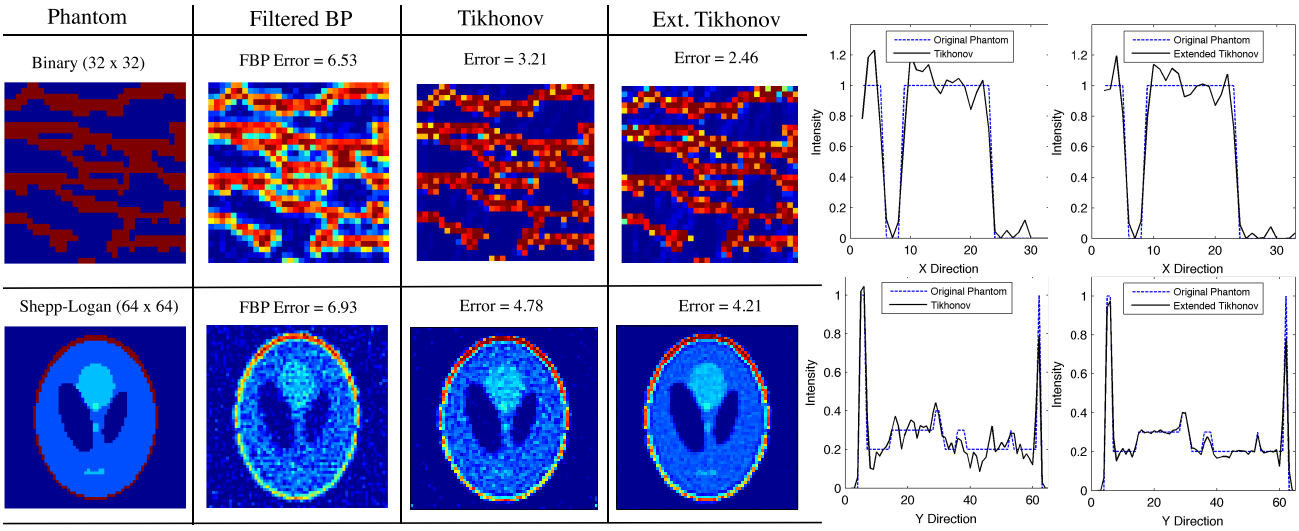

FIGURE 8. Comparative analysis of reconstructing a binary (relative noise = 0.05) and Shepp-Logan (relative noise = 0.1) phantom with Tikhonov and extended Tikhonov regularization. Intensity profiles of both phantoms show that extended Tikhonov performs better than Tikhonov. The optimization problem was was initialized from FBP and solved using an iterative forward-backward solver. Tikhonov reconstructions of the binary phantom were performed at a relatively lower regularization parameter to prevent smoothing.

TABLE 3. Comparative analysis of error rates for Tikhonov and extended Tikhonov reconstructions at varying relative noise and number of projections.

Phantom	Relative Noise	5%			10%			20%			50%		
	No. of Proj.	**36**	**18**	**9**	**36**	**18**	**9**	**36**	**18**	**9**	**36**	**18**	**9**
Smooth	Regular	5.19	9.46	11.31	12.87	14.18	16.63	18.61	27.49	34.54	68.46	77.38	82.37
	Extended	2.06	3.13	5.62	4.21	4.56	5.13	9.34	10.95	12.87	19.87	23.88	26.19
Shepp-Logan	Regular	3.98	4.35	5.28	4.78	7.34	8.94	8.17	10.46	16.56	17.74	20.71	32.84
	Extended	3.18	3.87	4.84	4.21	4.50	5.35	5.21	5.25	5.16	6.86	7.07	9.04
Binary	Regular	3.21	4.29	7.18	4.67	6.11	8.24	7.32	12.45	14.91	19.20	24.12	29.11
	Extended	2.46	2.98	3.30	3.09	4.12	4.36	6.71	8.43	9.88	11.61	14.28	18.29
Four-Phase	Regular	8.99	10.97	12.46	10.38	16.38	19.03	12.28	22.43	27.21	38.94	44.03	49.08
	Extended	6.32	7.11	8.40	9.11	10.49	12.26	11.90	15.38	18.43	22.19	26.46	29.15

extended field outside the ROI while reconstructing a density with TR.

We reconstructed a 64 × 64 binary phantom (relative noise = 0.05) and a 64 × 64 Shepp-Logan (relative noise = 0.1) using both TR and ETR. ETR simulations were conducted by zero-padding the sinogram corresponding to a 128 × 128 reconstruction (Fig. 8). The reconstructions were performed using a forward-backward iterative solver. In line with our findings for ART and SIRT, ETR performed better than TR when tested on a variety of phantoms under different noise conditions, as well as with varying numbers of total projections (Table 3). It is evident from these results that TR regularizes more powerfully than the methods discussed in the previous sections, thus the improvement due to the use of extended field is also significantly larger.

F. ADDITIONAL EXPERIMENTAL OBSERVATIONS

We observed that decreasing the field instead of extending it leads to having a reconstruction space smaller than corresponding projection size. On simulating several reconstructions by decreasing the field we observed that it always leads to a more erroneous reconstructions. This is the case if the error rate is calculated relative to the original phantom without excluding the region which was reduced by having a smaller field of view. That said, an extended field does not require an object to be fully enclosed in the ROI. If the object is not enclosed, *i.e.*, the sinogram is modified to reconstruct a part of the density, the projections still hold information about the removed part and the reconstruction / regularization method used will treat it as noise. On reconstructing partial densities from four different phantoms at different noise

levels we observed that an extended field always improved the error rate. This is the case if the error rate is calculated relative to the part of the phantom which was reconstructed. It should be noted that the major difference between Electron Lambda Tomography (ELT) [13] and extended field is that ELT targets the locality problem (*i.e.*, when the ROI does not contain the whole object), while it does not remove or redistribute noise like extended field does.

III. QUANTIFYING THE AMOUNT OF NOISE REMOVED

In this section we empirically analyze and quantify the amount of noise that redistributes into the extended region. This is essential to verify the effectiveness of extended reconstructions and allows us to quantify the amount of noise removed compared to the amount of noise added.

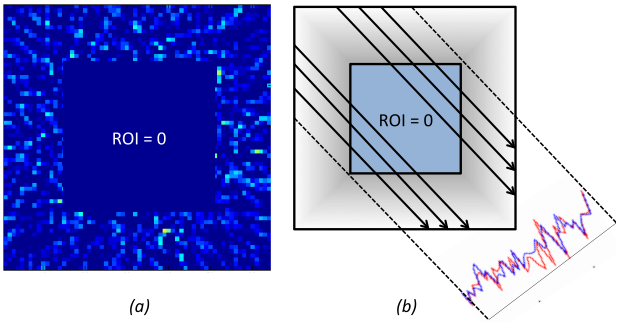

FIGURE 9. Experimental design to quantify the noise redistributed to the extended field. The pixels in the reconstructed ROI are set to zero and projections are taken relative to the ROI and compared with noise added to individual projections of the sinogram.

Experimental Setup: 36 projections were generated from a 64 × 64 Shepp-Logan Phantom and the resulting sinogram was corrupted with 15% added normalized random noise. The noisy sinogram was extended by zero-padding corresponding to a 128 × 128 reconstruction space. The resulting sinogram was reconstructed using ART (Kaczmarz), SIRT (Cimmino) and Tikhonov using FBP as the starting point. The 64 × 64 ROI in the resulting 128 × 128 extended reconstruction is set equal to zero (Fig. 9a). We then take 36 projections equivalent to the size of the ROI from this matrix (Figure 9b). This essentially means that we summed up pixel-by-pixel, all the noise removed from the ROI while leaving out regions that did not contribute to the original projections. These projections were then compared to the original noise added to each projection (Figure 10).

The good fit between the projected extended field region (blue curve in Fig. 10) and the noise added to the sinogram (red curve in Fig. 10) shows that most of the noise was redistributed to the extended region during regularization. Table 4 shows the average correlation between red and the blue signals. The fit for Tikhonov is better than SIRT and ART and the fit for SIRT is better than ART. This indicates that Extended Field works more powerfully for methods with a stronger regularization capability. Further results from similar simulations with SIRT, ART and Tikhonov are elaborated in the supplementary material.

TABLE 4. Average correlation between the noise redistributed to the extended region and the noise added.

Phantom	Rel. Noise	ART[1]	SIRT[2]	Tikhonov
Shepp-Logan	15%	0.6392	0.7026	0.7664
Shepp-Logan	30%	0.6894	0.7133	0.7911
Smooth	15%	0.3720	0.3914	0.5183
Smooth	30%	0.4781	0.5996	0.6215
Four-Phase	15%	0.3832	0.4419	0.4904
Four-Phase	30%	0.4189	0.5038	0.5617
Binary	15%	0.7162	0.7575	0.7924
Binary	30%	0.7592	0.7842	0.7966

[1] Kaczmarz Method
[2] Cimmino's Method

IV. ENHANCED REGULARIZATION USING EXTENDED FIELD

It is evident from experiments with algebraic methods (ART, SIRT and their variants) as well as with variational regularization (Tikhonov) that extended field enhances the effect of regularization. Extended field works better with stronger regularization methods and at higher noise levels e.g. extended field with Tikhonov regularization at 50% noise can improve the reconstruction several folds (Table 3, column 4). The distribution of the noise removed from Tikhonov reconstructions also fits much better with the actual noise added as compared to ART and SIRT (Table 4).

We reconstructed various phantoms using Tikhonov regularization for a changing regularization parameter (λ in Eq. 2) and observed that extended field reconstructions can achieve an enhanced regularization effect when compared to regular reconstructions at a relatively lower λ (Fig. 11). In accordance with our hypothesis the rationale behind this is the unique ability of an extra region to enhance the consistency of the solution with respect to the sinogram.

The regularization parameter controls the balance between the fit and the regularity of the solution. A large λ produces a strongly regular solution i.e. the solution is smoother. A lower λ produces a solution more faithful to the data (projections). Since having an extended field reduces the error at a relatively lower regularization parameter, this means that it can produce a solution which is more faithful to the data while preventing over-smoothing. The extended region allows for an increased fit between the projections (sinogram) and the reconstruction by achieving a better error rate at a lower λ.

V. OPTIMAL EXTENSION SIZE

Simulations in the previous sections show how extended field behaves with a variety of reconstruction methods, at various noise levels and at different number of projections. We show that extended field can have a promising effect on reconstructions by lowering the error rate and improving the correlation with the actual phantom. However, extending the sinogram to achieve an extra reconstruction space means increasing the size of the reconstruction problem which is a computational

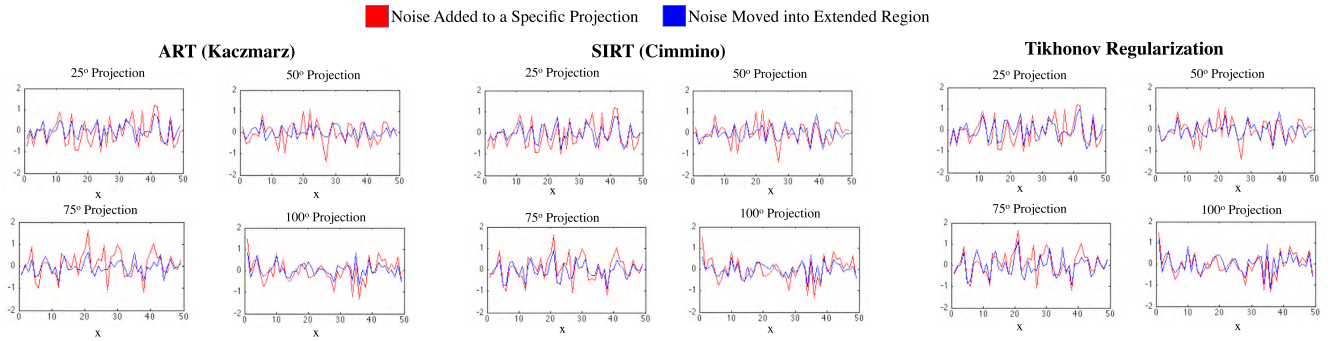

FIGURE 10. Comparison of noise removed, *i.e.*, noise redistributed into the extended field and the noise originally added to the projection at 25^o, 50^o, 75^o and 100^o for extended ART, SIRT and Tikhonov reconstructions of a Shepp-Logan phantom. The good fit shows that the amount of noise removed by the flexibility provided by the extended field is approximately equivalent to the amount of noise added while conducting the simulation (Table 4). Results for the entire sinogram and similar results for ART and SIRT have been presented in the supplementary material.

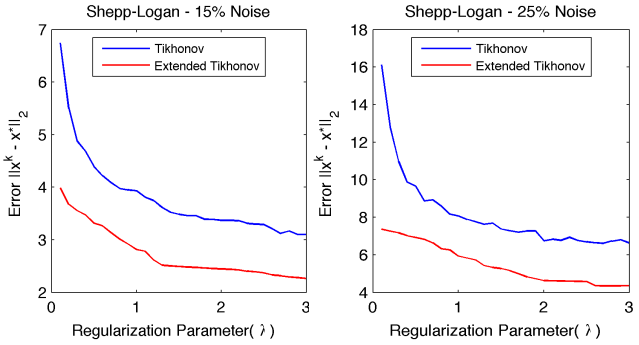

FIGURE 11. Comparative analysis of error rates for Tikhonov and Extended Tikhonov reconstructions at a varying regularization parameter ($0.1 \leq \lambda \leq 3$). The error rates are calculated corresponding to the ROI for Extended Tikhonov reconstructions. It can be seen that Extended Tikhonov achieves a much better error rate at a lower λ than regular Tikhonov.

constraint. Keeping this in mind, it is necessary to estimate an optimal extension size especially when dealing with real data.

We reconstructed 64×64 Shepp-Logan and Binary phantoms at varying extension steps (0, 2, 4, 8, . . . 512) and at different noise levels. Apart from these the experimental setup is the same as mentioned in the previous section. The binary phantom was reconstructed at a relatively lower regularization parameter to prevent smoothing. Fig. 12 summarizes these numerical tests and suggests that all extended reconstructions show a sharp decrease in the error rate during the first few extension steps followed by a saturation in error improvement. As the extended field is increased more and more noise is removed from the ROI into the extra region. However, extending the field can not continue to improve the ROI beyond a certain point. This is because extending the field can not remedy noise and inconsistence originating from missing data (*e.g.* less projections, missing wedge). It can be observed from the experiments that at higher noise levels the sharp decline in the error rate during the first few extension steps becomes much more prominent. Also, error rates for stronger variational regularization methods (Tikhonov) show a sharper decline when compared to mildly regularizing algebraic methods (ART, SIRT). After saturation the error rate stabilizes and varies only slightly despite large extension sizes.

Extremely large extension steps lead to a slight increase in the error rate. For example extending a 64×64 Shepp-Logan phantom corresponding to a 4096×4096 reconstruction gives an error of 4.268 as compared to a 256×256 reconstruction which yields an error rate of 4.257. Moreover, the extended field reconstruction of phantoms with no noise added leads to extremely slight improvements in the error rate, as mentioned inconsistencies due to missing data can not be corrected, the slight improvement comes form the correction of errors originating from the numerical treatment of the problem.

The optimal extension size depends on the type of raw data, the amount of noise and the regularization capability of the reconstruction method. As shown by our experiments a strong regularization method will need a smaller extension to remove most of the noise from the ROI into the extended region. For instance, reconstructions in [19] were performed using ART, which has mild regularization capabilities, and in that specific case twice the reconstruction size may have been needed. When using Tikhonov regularization an extension of half the size of the actual phantom, removes most of the noise. Contrary to [19] we observed that extending the reconstruction space twice or more the actual reconstruction space is not necessary to realize the full potential of an extended field. The ratio of error improvement to extension size decreases at higher extensions. It is computationally inefficient to increase the extension size beyond half the size of the actual reconstruction if a powerful enough regularization method is employed, since the gain in SNR beyond that is not significant.

In short, the optimal and most computationally efficient extension size can be decided depending on the type of data being reconstructed, the amount of noise in the data, the number of projections and more importantly the regularization capabilities of the reconstruction method being used. When dealing with real data the optimal extension size can be

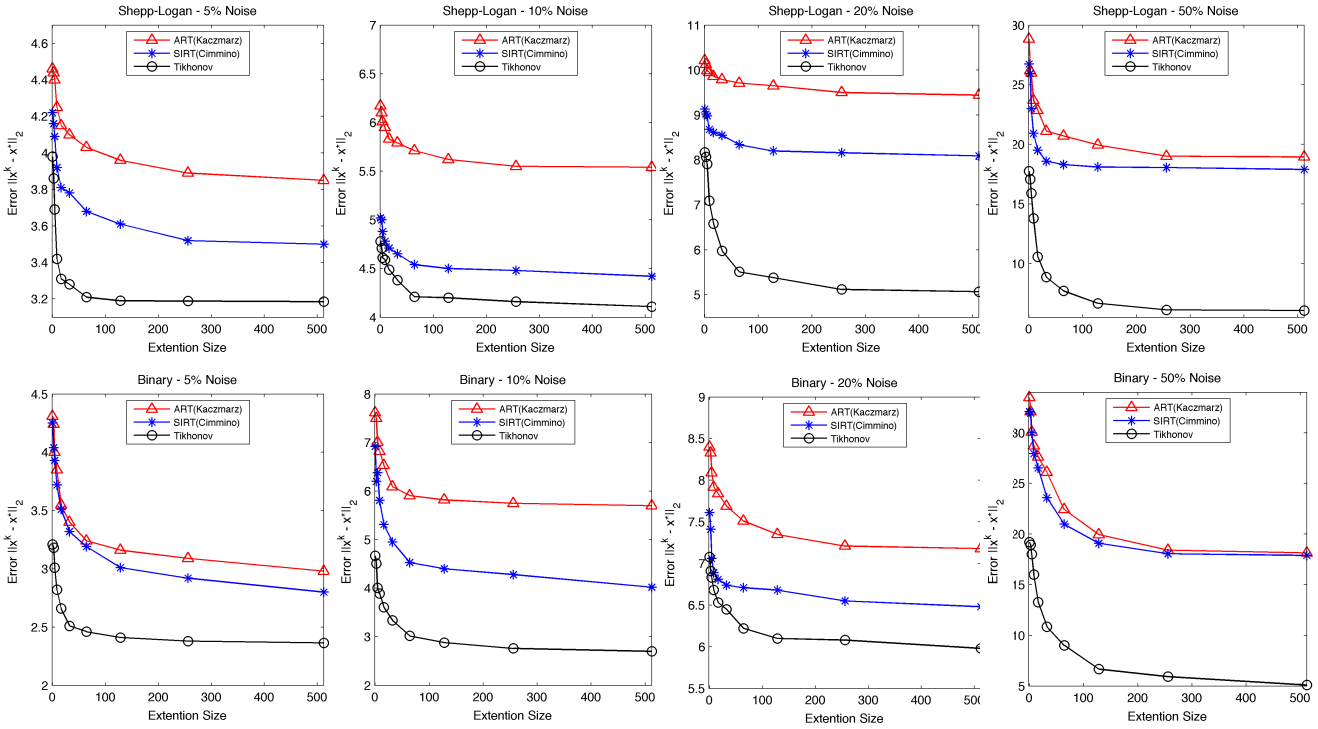

FIGURE 12. Comparative analysis of error rates for ART, SIRT and Tikhonov reconstructions at varying extension steps 0, 2, 4, 8, . . . 512 starting from a 64 × 64 phantom. It can be seen that most of the benefit of an extended field is achieved if the size of the extension is half the actual reconstruction size. All reconstructions show a sharp improvement during the first few small extension steps followed by a saturation of error improvement for larger extensions.

tuned for a specific imaging device and correlated with data collection variables such as number of projections and the dose used etc.

VI. EXPERIMENTAL RESULTS FROM 3D DATA

The previous sections showed the effect of an extended field when reconstructing simulated 2D images from 1D projections. This section elaborates the effects of reconstructing 3D densities from 2D data with an extra region outside the ROI. In 3D, the reconstruction problem generally becomes considerably more complicated. For real-data, deconvolution of the point spread function (PSF) is required to obtain accurate reconstructions. Problems due to missing data (missing wedge) are also much more prominent. We reconstructed the structure of an inorganic nano-particle and a membrane protein to demonstrate the effectiveness of extended field in reconstructing real 3D data. We used our in-house constrained maximum entropy tomography (COMET) reconstruction package [7] for reconstructing from the 2D TEM data, since it has built-in PSF deconvolution and regularization.

Consider the z-axis to be the direction of the electron beam of the Cryo-Electron Microscope when the data was collected. Let Z_{ROI} be the size of z for which the 3D reconstruction is desired, *i.e.*, the ROI. For the purpose of testing, COMET-based reconstructions can be iterated for volumes increasing in the z-direction, such that $Z_1 < Z_2 < Z_3 < \ldots < Z_n$, resulting in n-many 3D reconstructions. Each successive reconstruction has an increased volume in the z-direction (Fig. 13). Reconstructions in higher volumes are expected to remove more noise out of the ROI. Finally the ROI is extracted from each of these reconstructions and a comparison is made with the original reconstruction. It should be noted that multiple reconstructions with increasing Z are only for testing the amount of noise removed is relative to extension size. Practically, the method can simply be used by reconstructing a single volume larger than the ROI.

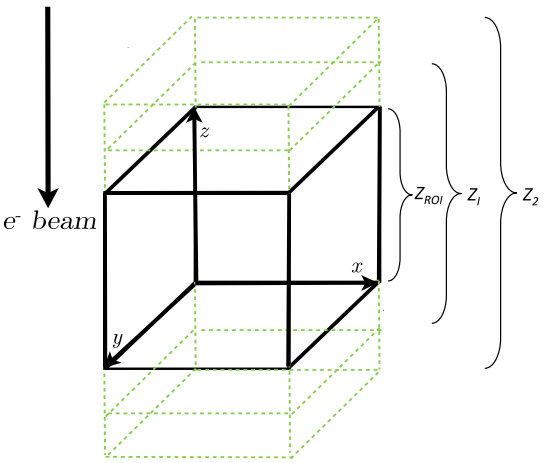

FIGURE 13. Figure showing successive reconstructions on a large volume by increasing in z-direction (*i.e.*, reconstructions with an extended field).

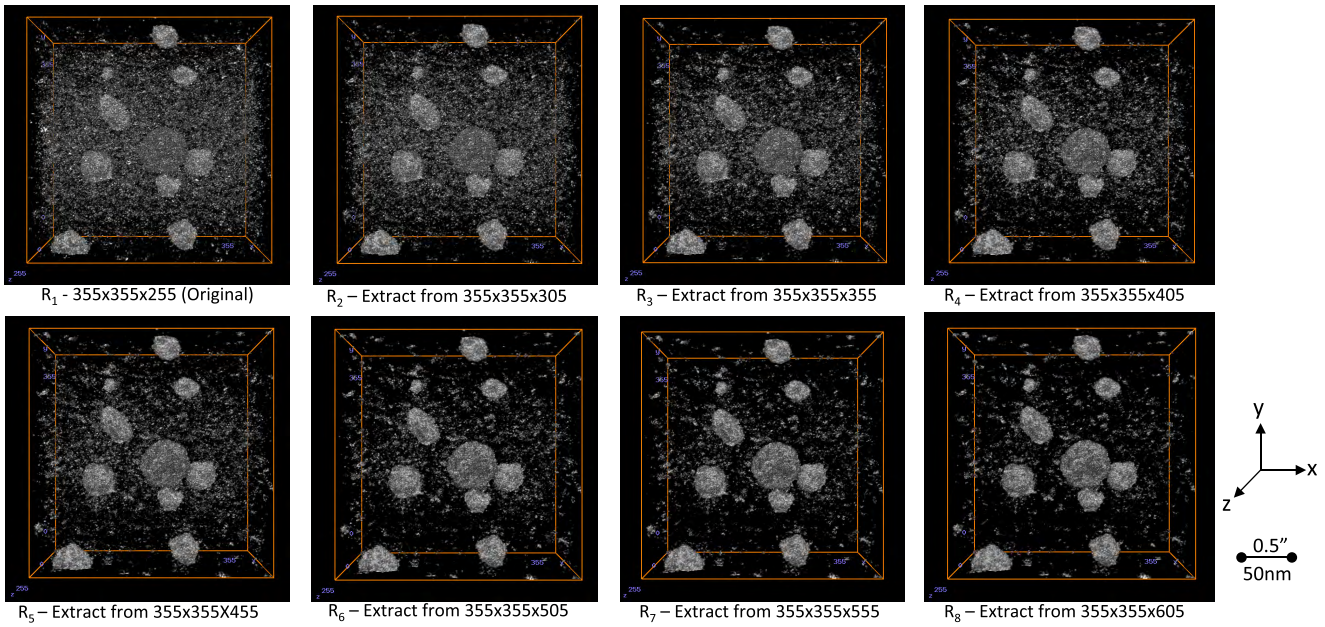

FIGURE 14. Extracted ROIs (355 × 355 × 255) of successive reconstructions of a colloidal silica sample with increasing z. Reconstructions with an extended field (*i.e.* $R_2 - R_8$) have a lower noise within the ROI. The map grid size for one pixel is 5.626Å and the average size of a colloidal silica nano-particle is 31.5nm. The large particle in the center of the reconstruction has lower density as compared to the smaller particles because it is water in the form of crystallized ice. Videos can be viewed in the multimedia supplement with this paper.

A. SAMPLE: COLLOIDAL SILICA

Colloidal silica is made of synthetically manufactured SiO_2 nanoparticles. Like large proteins, it has a diameter of 25-70 nm and a density of 1.28 g/cm^3, displaying scattering properties comparable to those of proteins [41]. There are several advantages to using colloidal silica as a test object. Since colloidal silica is an inorganic sample it suffers minimally from degradation due to electron beam exposure during data collection. A higher electron dose can be given to such a sample, reducing the shot noise. The colloidal silica sample used here is typically used in paint: BINDZIL of grade 40/130 and was kindly provided by Eka Chemicals, Akzo Nobel, Sweden. Data was collected using a Philips CM200 200keV FEG transmission electron microscope (TEM). The specimen was tilted between ±65° and micrographs were recorded on a CCD detector (F224, TVIPS Gmbh, Germany) every other degree. Eight 3D COMET reconstructions were performed starting with grid points 355 × 355 × 255 (*i.e.*, dimensions in x,y and z axis respectively) to 355 × 355 × 605 with Z increasing incrementally by 50 grid points. Then the common region 355 × 355 × 255 was extracted from all these reconstructions (Fig. 14). Images were adjusted to the same contrast threshold. We observe that the background noise decreases over successive reconstructions. Fig. 15 shows an intensity profile of a single line through a slice of the 3D reconstruction at two different values of Z. At a higher value of Z, the signal is much stronger compared to the noise. Similar results can be achieved by increasing the volume in the y-direction or in both the z- and y-directions. However, the reconstruction space cannot be increased by increasing the x-direction since the sample is tilted around this axis.

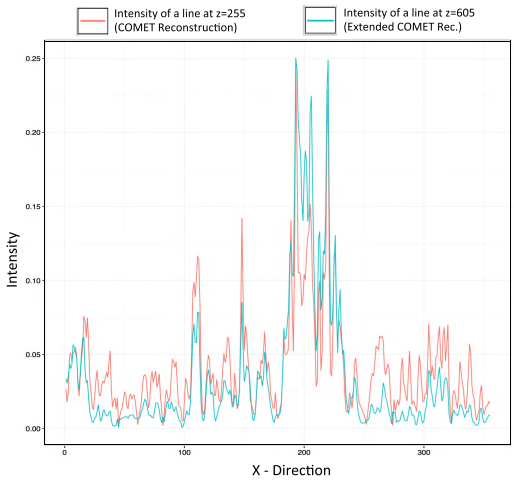

FIGURE 15. Intensity profiles of a single line through a slice of the 3D reconstruction at two different extension values. The peak represents the signal (*i.e.* a silica nano-particle). For a reconstruction with an extended field the signal within the ROI is significantly stronger as compared to the noise.

B. SAMPLE: P. falciparum ERYTHROCYTE MEMBRANE PROTEIN 1 (PfEMP1)

Similar to the colloidal silica reconstructions we reconstructed the structure of *P. falciparum* Erythrocyte Membrane Protein 1 (*PfEMP1*) with and without extension of the field (Fig. 16). A more detailed account of the sample preparation, structure and properties of the 280kD ectodomain of this membrane protein can be found in [28]. The data was collected on a Titan Krios 300kV with a FEI Falcon II camera with 14 micron pixels. 281 micrographs were recorded spaced 0.5 degrees apart. The effective magnification was 61756 giving a pixel-size of 2.267Å. The total dose used was approximately 40 electrons/Å^2, or 0.14 electrons/Å^2

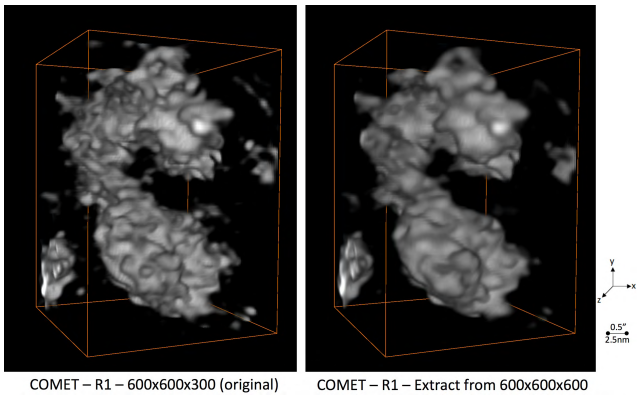

FIGURE 16. Extracts (70 × 100 × 70) from 3D reconstructions of P. *falciparum* Erythrocyte Membrane Protein 1 (PfEMP1) without (600 × 600 × 300) and with (600 × 600 × 600) extension of the field. The extended reconstruction shows less noise as compared to the regular reconstruction. Pixel size is 2.267Å.

per image. The volume of the original reconstruction was 600 × 600 × 300 and that of the extended reconstruction was 600 × 600 × 600. The results have been presented in Fig. 16 and show a clear improvement in the quality of the reconstruction using extended field. Both reconstructions were low-pass filtered to 15Å resolution.

VII. LIMITATIONS AND SHORTCOMINGS

Limitations of using an extended field during tomographic reconstructions can be summarized as follows:

- Extended field does not work with filtered back projection and its variants. Such methods do not allow for redistribution of noise into an extended region. For an analytical method having an extended region outside the ROI would simply mean the same intensity values being distributed along a longer ray path.
- Extended field does not correct for inconsistencies arising from missing data due to limited number of projections or the missing wedge. Although, noise removal due to an extended field might aid other methods which can correct for missing data such as [7].
- The method behaves poorly with weaker regularization methods, better results can be achieved by using more powerful regularization methods.
- Extended field does not work in cases where an alternative, consistent but incorrect solution can be found. Although this would be a rare case, it remains a possibility.

VIII. CONCLUSIONS

In this paper we show that extending the reconstruction field during iterative image reconstruction can render better results when compared to non-extended reconstructions. This principle was tested with extensive simulations using a variety of reconstruction methods. We empirically validate that solutions from extended reconstructions preserve a better fit to the collected projection data at a lower regularization parameter. We also verify the effectiveness of this method by fitting the noise removed and noise added during simulations. We further strengthened our claims by testing on real cryo-ET data collected from an inorganic colloidal silica and a biological *PfEMP1* sample. The technique is unique but it can segregate the signal from noise without significantly interfering directly with the signal since it does not involve manipulating individual reconstructed voxels using standard filtering, or post-processing procedures, which may remove high-frequency details from the reconstruction. Moreover, this method is general and can be extended to be used with other tomographic modalities.

ACKNOWLEDGMENT

The authors would like to thank Dr. Steven D. Aird for language assistance and Shizuka Kuda for logistical arrangements. Samples of BINDZIL (Colloidal Silica) were donated by Eka Chemicals, Akzo Nobel, Sweden.

DISCLOSURE

Parts of this work have been filed for a US patent under US 14/770,245 and PCT patent under PCT/JP2014/001214 by Okinawa Institute of Science and Technology (OIST) School Corporation, Okinawa, Japan.

REFERENCES

[1] J. Elands and U. Skoglund, "Cryo electron microscopy and electron tomography will play a crucial role in the future of drug development," *Drug Discovery*, pp. 80–85, 2005.
[2] H. R. Saibil, "Macromolecular structure determination by cryo-electron microscopy," *Acta Crystallogr. Sec. D, Biol. Crystallogr.*, vol. 56, no. 10, pp. 1215–1222, 2000.
[3] D. Fanelli and O. Öktem, "Electron tomography: A short overview with an emphasis on the absorption potential model for the forward problem," *Inverse Problems*, vol. 24, no. 1, p. 013001, Feb. 2008.
[4] S. Sandin, L.-G. Öfverstedt, A.-C. Wikström, Ö. Wrange, and U. Skoglund, "Structure and flexibility of individual immunoglobulin G molecules in solution," *Structure*, vol. 12, no. 3, pp. 409–415, Mar. 2004.
[5] A. J. Koster *et al.*, "Perspectives of molecular and cellular electron tomography," *J. Struct. Biol.*, vol. 120, no. 3, pp. 276–308, Dec. 1997.
[6] Y. Censor, "Finite series-expansion reconstruction methods," *Proc. IEEE*, vol. 71, no. 3, pp. 409–419, Mar. 1983.
[7] U. Skoglund, L.-G. Öfverstedt, R. M. Burnett, and G. Bricogne, "Maximum-entropy three-dimensional reconstruction with deconvolution of the contrast transfer function: A test application with adenovirus," *J. Struct. Biol.*, vol. 117, no. 3, pp. 173–188, Nov. 1996.
[8] R. A. Crowther, D. J. DeRosier, and A. Klug, "The reconstruction of a three-dimensional structure from projections and its application to electron microscopy," *Proc. R. Soc. Lond. A, Math. Phys. Sci.*, vol. 317, no. 1530, pp. 319–340, Jun. 1970.
[9] O. Öktem, "Mathematics of electron tomography," in *Handbook of Mathematical Methods in Imaging*. Springer, 2015, pp. 937–1031.
[10] J.-J. Fernandez, "Computational methods for electron tomography," *Micron*, vol. 43, no. 10, pp. 1010–1030, Oct. 2012.
[11] Z. Saghi *et al.*, "Compressed sensing electron tomography of needle-shaped biological specimens—Potential for improved reconstruction fidelity with reduced dose," *Ultramicroscopy*, vol. 160, pp. 230–238, Jan. 2016.
[12] R. A. Brooks and G. Di Chiro, "Theory of image reconstruction in computed tomography," *Radiology*, vol. 117, no. 3, pp. 561–572, Dec. 1975.
[13] E. T. Quinto, U. Skoglund, and O. Öktem, "Electron lambda-tomography," *Proc. Nat. Acad. Sci. USA*, vol. 106, no. 51, pp. 21842–21847, 2009.
[14] R. Gordon, R. Bender, and G. T. Herman, "Algebraic reconstruction techniques (ART) for three-dimensional electron microscopy and X-ray photography," *J. Theor. Biol.*, vol. 29, no. 3, pp. 471–481, 1970.

[15] P. Gilbert, "Iterative methods for the three-dimensional reconstruction of an object from projections," *J. Theor. Biol.*, vol. 36, no. 1, pp. 105–117, Jul. 1972.

[16] A. Brandt, "Algebraic multigrid theory: The symmetric case," *Appl. Math. Comput.*, vol. 19, nos. 1–4, pp. 23–56, Jul. 1986.

[17] G. Cimmino and Consiglio Nazionale delle Ricerche, *Calcolo Approssimato per le Soluzioni dei Sistemi di Equazioni Lineari*. Istituto per le applicazioni del calcolo, 1938.

[18] Y. Censor, "Row-action methods for huge and sparse systems and their applications," *SIAM Rev.*, vol. 23, no. 4, pp. 444–466, Oct. 1981.

[19] R. A. Crowther and A. Klug, "Three dimensional image reconstruction on an extended field—A fast, stable algorithm," *Nature*, vol. 251, no. 5475, pp. 490–492, Oct. 1974.

[20] A. Tikhonov, "Solution of incorrectly formulated problems and the regularization method," *Sov. Math. Dokl.*, vol. 5, pp. 1035–1038, Nov. 1963.

[21] Y. Deng, Y. Chen, Y. Zhang, S. Wang, F. Zhang, and F. Sun, "ICON: 3D reconstruction with 'missing-information' restoration in biological electron tomography," *J. Struct. Biol.*, vol. 195, no. 1, pp. 100–112, Jul. 2016.

[22] Z. Saghi *et al.*, "Three-dimensional morphology of iron oxide nanoparticles with reactive concave surfaces. a compressed sensing-electron tomography (CS-ET) approach," *Nano Lett.*, vol. 11, no. 11, pp. 4666–4673, 2011.

[23] R. Leary, Z. Saghi, P. A. Midgley, and D. J. Holland, "Compressed sensing electron tomography," *Ultramicroscopy*, vol. 131, pp. 70–91, Aug. 2013.

[24] M. D. Guay, W. Czaja, M. A. Aronova, and R. D. Leapman, "Compressed sensing electron tomography for determining biological structure," *Sci. Rep.*, vol. 6, Jun. 2016, Art. no. 27614.

[25] H. Rullgård, O. Öktem, and U. Skoglund, "A componentwise iterated relative entropy regularization method with updated prior and regularization parameter," *Inverse Problems*, vol. 23, no. 5, pp. 2121–2139, Oct. 2007.

[26] L. Bongini, D. Fanelli, F. Piazza, P. De Los Rios, S. Sandin, and U. Skoglund, "Freezing immunoglobulins to see them move," *Proc. Nat. Acad. Sci. USA*, vol. 101, no. 17, pp. 6466–6471, Apr. 2004.

[27] J. Wartiovaara *et al.*, "Nephrin strands contribute to a porous slit diaphragm scaffold as revealed by electron tomography," *J. Clin. Invest.*, vol. 114, no. 10, pp. 1475–1483, Nov. 2004.

[28] R. Akhouri, S. Goel, H. Furusho, U. Skoglund, and M. Wahlgren, "Architecture of human IgM in complex with *P. falciparum* erythrocyte membrane protein 1," *Cell Rep.*, vol. 14, no. 4, pp. 723–736, Feb. 2016.

[29] P. C. Hansen, *Discrete Inverse Problems: Insight and Algorithms*, vol. 7. Philadelphia, PA, USA: SIAM, 2010.

[30] G. H. Golub, P. C. Hansen, and D. P. O'Leary, "Tikhonov regularization and total least squares," *SIAM J. Matrix Anal. Appl.*, vol. 21, no. 1, pp. 185–194, 1999.

[31] C. D. Meyer, *Matrix Analysis and Applied Linear Algebra*, vol. 2. Philadelphia, PA, USA: SIAM, 2000.

[32] P. C. Hansen and M. Saxild-Hansen, "AIR tools—A MATLAB package of algebraic iterative reconstruction methods," *J. Comput. Appl. Math.*, vol. 236, no. 8, pp. 2167–2178, 2012.

[33] A. Björck and T. Elfving, "Accelerated projection methods for computing pseudoinverse solutions of systems of linear equations," *BIT Numer. Math.*, vol. 19, no. 2, pp. 145–163, 1979.

[34] L. A. Shepp and B. F. Logan, "The Fourier reconstruction of a head section," *IEEE Trans. Nucl. Sci.*, vol. NS-21, no. 3, pp. 21–43, Jun. 1974.

[35] Y. Censor and T. Elfving, "Block-iterative algorithms with diagonally scaled oblique projections for the linear feasibility problem," *SIAM J. Matrix Anal. Appl.*, vol. 24, no. 1, pp. 40–58, 2002.

[36] Y. Censor, T. Elfving, G. T. Herman, and T. Nikazad, "On diagonally relaxed orthogonal projection methods," *SIAM J. Sci. Comput.*, vol. 30, no. 1, pp. 473–504, 2008.

[37] T. Elfving, T. Nikazad, and C. Popa, "A class of iterative methods: Semi-convergence, stopping rules, inconsistency, and constraining," Linköping Univ., Linköping, Sweden, Tech. Rep., 2010.

[38] T. Elfving, T. Nikazad, and P. C. Hansen, "Semi-convergence and relaxation parameters for a class of SIRT algorithms," *Electron. Trans. Numer. Anal.*, vol. 37, pp. 321–336, 2010.

[39] L. Landweber, "An iteration formula for fredholm integral equations of the first kind," *Amer. J. Math.*, vol. 73, no. 3, pp. 615–624, Jul. 1951.

[40] Y. Censor, D. Gordon, and R. Gordon, "Component averaging: An efficient iterative parallel algorithm for large and sparse unstructured problems," *Parallel Comput.*, vol. 27, no. 6, pp. 777–808, May 2001.

[41] T. Mizutani, K. Arai, M. Miyamoto, and Y. Kimura, "Application of silica-containing nano-composite emulsion to wall paint: A new environmentally safe paint of high performance," *Prog. Org. Coatings*, vol. 55, no. 3, pp. 276–283, Mar. 2006.

FAISAL MAHMOOD received the Ph.D. degree in biomedical imaging from the Okinawa Institute of Science and Technology, Japan, in 2017. He is currently a Post-Doctoral Fellow with the Department of Biomedical Engineering, Johns Hopkins University, Baltimore, MD, USA. His research interests involve machine learning and high-performance computing for biomedical imaging applications.

LARS-GÖRAN ÖFVERSTEDT received the Ph.D. degree from Uppsala University, Sweden, in 1983. In 1992, he joined Prof. U. Skoglund as a Researcher with Karolinska Institutet, Stockholm, Sweden. Since 2010, he has been a Staff Scientist with the Structural Cellular Biology Unit, Okinawa Institute of Science and Technology Graduate University, Okinawa, Japan.

MÄRT TOOTS received the B.Sc. and M.Sc. degrees in statistics from the University of Tartu in 2008 and 2012, respectively, with a focus on applying probability theory on sequence alignment problems, and the Ph.D. degree from the Okinawa Institute of Science and Technology under the supervision of Prof. U. Skoglund, with a focus on the development of methodology for imaging protein nanocrystals using electron tomography.

GUNNAR WILKEN received the Diplom, Ph.D., and Docent degrees from the University of Münster, Germany, in 1998, 2004, and 2011, respectively. He is currently a Staff Scientist with the Okinawa Institute of Science and Technology, Japan. His research interests include inverse problems and mathematical logic.

ULF SKOGLUND received the Ph.D. degree from Stockholm University, Sweden, in 1969. He was a Professor with the Karolinska Institutet, Stockholm, Sweden, from 1996 to 2009. Since 2010, he has been a Professor with the Structural Cellular Biology Unit, Okinawa Institute of Science and Technology, Okinawa, Japan. He has developed electron-tomographic technologies allowing for images of proteins to be generated so that structures can be fitted into the 3-D densities. This technique is called constrained maximum entropy tomography. His unit has also developed a large-scale dynamics method that allows for quantitative calculations of molecular movements in solution. His current developments concern the mathematics and improvements of basic 3-D reconstruction principles and also on reconfigurable and high-performance computing.